Temperature-Induced Switchable Adhesion using Nickel–Titanium–Polydimethylsiloxane Hybrid Surfaces

*Mareike Frensemeier, Jessica S. Kaiser, Carl P. Frick, Andreas S. Schneider, Eduard Arzt, Ray S. Fertig III, and Elmar Kroner**

A switchable dry adhesive based on a nickel–titanium (NiTi) shape-memory alloy with an adhesive silicone rubber surface has been developed. Although several studies investigate micropatterned, bioinspired adhesive surfaces, very few focus on reversible adhesion. The system here is based on the indentation-induced two-way shape-memory effect in NiTi alloys. NiTi is trained by mechanical deformation through indentation and grinding to elicit a temperature-induced switchable topography with protrusions at high temperature and a flat surface at low temperature. The trained surfaces are coated with either a smooth or a patterned adhesive polydimethylsiloxane (PDMS) layer, resulting in a temperature-induced switchable surface, used for dry adhesion. Adhesion tests show that the temperature-induced topographical change of the NiTi influences the adhesive performance of the hybrid system. For samples with a smooth PDMS layer the transition from flat to structured state reduces adhesion by 56%, and for samples with a micropatterned PDMS layer adhesion is switchable by nearly 100%. Both hybrid systems reveal strong reversibility related to the NiTi martensitic phase transformation, allowing repeated switching between an adhesive and a nonadhesive state. These effects have been discussed in terms of reversible changes in contact area and varying tilt angles of the pillars with respect to the substrate surface.

1. Introduction

Many industrial processes require efficient adhesion systems to grip and release fragile objects such as wafers, lenses or glass plates. State-of-the-art solutions such as vacuum-based handling systems are cost intensive and have limitations in their applicability. An alternative are micropatterned dry adhesive surfaces similar to those found in nature in various organisms. Several studies, inspired by adhesion systems of spiders and geckos, have investigated synthetic micropatterned adhesives.[1] These structures allow easy adaptation to a wide variety of surfaces, causing an increase in contact area at negligible elastic strain and, thus, improved adhesion.

One significant barrier for the application of micropatterned surfaces is the lack of switchability. For gecko setae, the fibrillar structures can be detached by a combination of shear- and peel-motion.[2] While it is possible to mimic the design of the gecko structures, the complex detachment mechanism is often impractical or expensive for implementation into industrial processes.[3] A system showing switchable adhesion will be of industrial interest as it might be capable of replacing suction systems, allow handling of fragile and sensitive objects, and can even be used in a wide variety of conditions including in vacuum.

Several studies have investigated various approaches to generate switchable adhesion. Vogel and Steen used surface tension force from liquid bridges which could be controlled by a low-voltage pulse, driving an electro-osmotic flow to generate switchable adhesion.[4] Due to the use of a liquid film and its capillary forces this system is not applicable in vacuum or for very sensitive and clean products, where residual free adhesion is required.

Other studies have focused on magnetic concepts for switchable dry adhesion.[5] Northen et al. developed a hybrid-material of an adhesive polymer combined with magnetic nickel cantilevers. They used a magnetic field as trigger and were able to change the orientation of the cantilevers by magnetic fields, which induced a change in contact area and, thus, in adhesion.[6] Although the system showed good switchability, the adhesion forces were very small. Paretkar et al. presented a pressure actuated adhesive system, where adhesion can be switched by varying the compressive load.[7] Mechanical overloading caused buckling of the structures and subsequent loss of intimate contact, which resulted in adhesion loss when a threshold compressive load was applied. This system is sensitive to shear movement, which might trigger the buckling and subsequently loss in adhesion. Another switchable adhesive system, based on a change in contact area and crack-trapping, was presented by Nadermann et al.[8] A metastable film-terminated architecture is switched via air pressure between a collapsed and

M. Frensemeier, Prof. E. Arzt
Saarland University
Campus D 2 2, 66123 Saarbrücken, Germany
M. Frensemeier, J. S. Kaiser, Dr. A. S. Schneier, Prof. E. Arzt, Dr. E. Kroner
INM – Leibniz Institute for New Materials
Campus D 2 2, 66123 Saarbrücken, Germany
E-mail: elmar.kroner@inm-gmbh.de
Dr. C. P. Frick, Dr. R. S. Fertig III
Department of Mechanical Engineering
University of Wyoming
Department 3295, 1000 E University Ave
Laramie, WY 82071, USA

DOI: 10.1002/adfm.201500437

uncollapsed state; the two states lead to different adhesive properties. The change of the surface state was induced by mechanical loading or air pressure, and the associated critical values were unknown. Triggering this system by use of air pressure may restrict its applicability for use in vacuum. Jeong et al. also used mechanical loading or stretching as a trigger to switch adhesion in a wrinkled dry adhesive surface.[9] Other systems showing switchable adhesion are based on shape memory polymers. Due to a specific external stimulus like light or temperature a phase change in the material occurs and leads to a switch of the stiffness, geometry or surface properties.[10,11] A drawback of these systems is their reversibility. Many systems show a characteristic switch of their properties after applying the specific trigger but need another external force to return back to their initial state.[12] Thus, the combination of two stimuli such as mechanical deformation and thermal-induced recovery are frequently used.[11–13] Reddy et al. used a micropatterned shape-memory polymer to change adhesion. However, this required shearing of the pillars to change the contact area and consequently the deformation of the polymer was irreversible.

NiTi alloys can be trained to elicit a reversible two-way shape-memory effect, where the shape can be spontaneously changed between a high and a low temperature state.[14] It was shown that indentation followed by planarization yields a shape-memory surface, where the topography of the NiTi surface reversibly changed from flat to bumpy by heating above, or cooling below, the austenite-martensite phase transformation temperatures.[15,16] The fundamental premise is that the localized deformation due to indentation leads to the two-way shape-memory effect (TWSME). A more recent study has strongly indicated that the mechanism associated with this is deformation-stabilized martensite.[17] It is assumed that by acting as a nucleation site the deformation-stabilized martensite guides the growth of the thermally induced martensite and, consequently, the shape change during cooling. This effect has been shown to be repeatable over thermal cycling.

The present work combines the NiTi with TWSME as a functional backing layer with an adhesive polydimethylsiloxane (PDMS) top layer to achieve temperature-induced switchable adhesion. The smooth or patterned PDMS layer functions as adhesion mediating contact element. The deformation-induced TWSME is used to control the topography of the surface and, thus, the contact area of the adhesive.

2. Results and Discussion

In this study, we used a polycrystalline alloy with a nominal composition of Ti-50.3 at% Ni with an austenite finish temperature of 76 °C and a martensite finish temperature of 25 °C. Thus, the material is expected to be martensitic at room temperature, and austenitic in the heated state at 80 °C and above. At temperatures in between, both states are stable depending on the thermal history of the material. The TWSME was trained using an approach similar to that outlined by Fei et al.[16] and more recently by Qin et al.,[17] where semi-hemispherical protrusions are created using indentation. The plastically deformed surfaces were planarized by grinding and polishing. Subsequent heating above the austenite start temperature led to the formation of surface protrusions. Two different hybrid systems were fabricated using the indented and planarized NiTi samples: systems covered with a smooth 10–15 μm thick layer of PDMS and systems coated with a patterned PDMS layer having hexagonal arrays of pillars with 50 μm diameter and a height of 40 μm.

The sample topography was characterized in the cooled (flat) state at room temperature and in the heated (structured) state at 80 °C using an optical and white light interferometric microscope equipped with a heating stage (**Figure 1**). Figure 1a shows an optical image of the sample consisting of a thin layer of PDMS cast directly onto the TWSME NiTi surface in the flat state. Figure 1c,e shows the same sample when heated to the structured state. Similarly, Figure 1b,d,f) shows the sample with structured PDMS pillars cast onto a duplicate NiTi surface, in both the flat and bumpy states.

The smooth sample shows protrusions in the heated state with an average and standard deviation height of 4.0 ± 0.3 μm and a center-to-center distance of about 400 μm (Figure 1c,e). The protrusions were entirely reversible after cooling. For the sample with the patterned PDMS layer the pillars and the underlying protrusions are clearly visible in the heated state (Figure 1d,f). Thus, the topographic change of the NiTi can be observed also on the PDMS layer.

2.1. Adhesive Performance and Reversibility

The adhesive properties were measured 15 times at three different positions for multiple temperatures, by load-displacement tests. The sample was brought into contact with a spherical probe, loaded and unloaded again while continuously measuring forces. The maximum load is called preload and the minimum (negative) load is defined as the pull-off force ($F_{C.}$). Experiments were performed at temperatures ranging from room temperature up to 100 °C in steps of 20 °C, using a constant displacement velocity. Note that the different *x*-axis scaling in **Figure 2**b is due to differing stiffness of the spring used in the measurement system. The displacement is including cantilever and sample.

Figure 2a,b shows the load-displacement curves in the heated and cooled state, showing the overall displacement in the system. For the sample with the smooth PDMS layer, the average pull-off force at room temperature is 1142 ± 113 μN, and decreases to 574 ± 17 μN after heating to 80 °C. The patterned sample shows an average pull-off force of 711 ± 27 μN in the cooled state and nearly no adhesion in the heated state, respectively. Upon unloading multiple detachment events lead to several detachment-peaks, which are typical for structured surfaces if tested with spherical probes.[18,19]

Adhesion measurements were performed for ten temperature cycles to investigate the reversibility of the shown effects. The results in Figure 2c,d indicate no significant loss in adhesion and the switching performance for both hybrid systems. While the patterned sample switches continuously between "on" and "off", the adhesion of the sample with the smooth PDMS layer drops to 54% of the initial pull-off force at room temperature. The velocity of switching is restricted by heating and cooling, since the transition of the topography

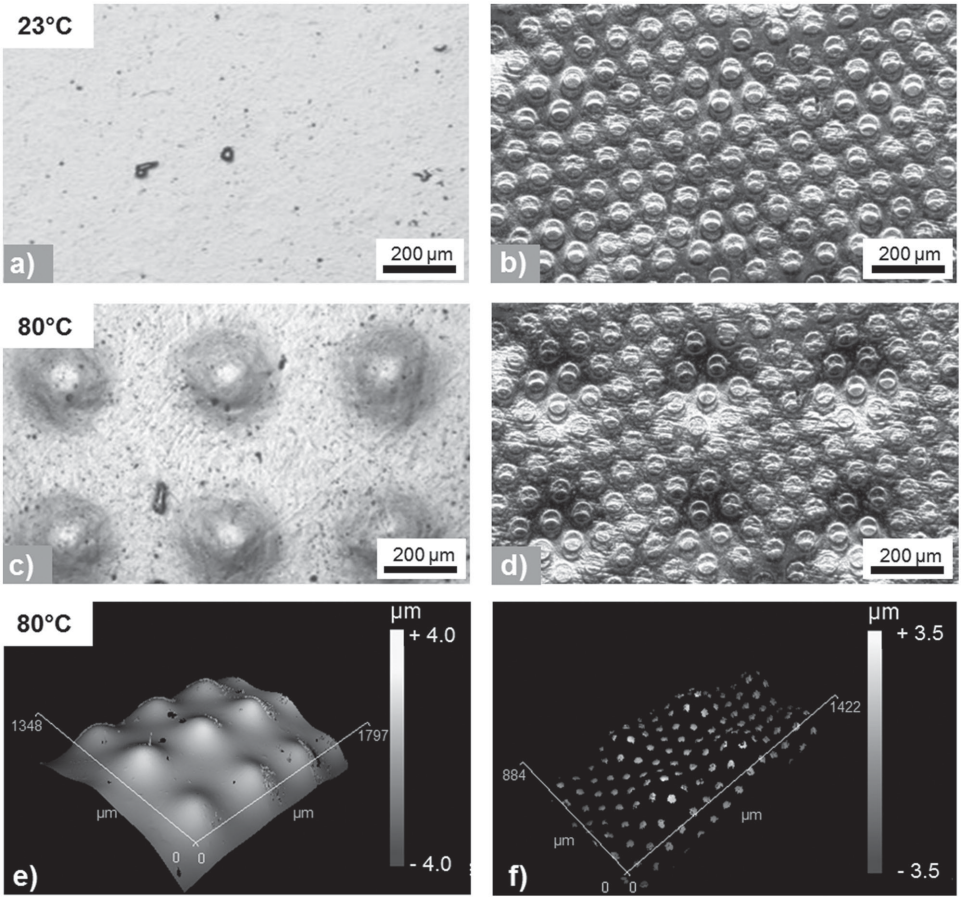

Figure 1. Topographic change of the surface for the two NiTi-PDMS hybrid systems with a smooth PDMS layer (left column) and patterned PDMS layer (right column). a,b) At room temperature (23 °C) both systems are in a flat state. c,d) In the heated state (80 °C) both systems show a characteristic surface structure induced by the TWSME in the NiTi surface. Pictures are taken via optical microscopy. e,f) The topography in the heated state, imaged and quantified by white light interferometry.

switches instantaneous once the transformation temperature is reached.

For better comparability a switching efficiency S is defined as

$$S = 1 - \frac{F_{CB}}{F_{CF}} \tag{1}$$

where F_{CF} is the pull-off force in the flat (adhesive, room temperature) state, and F_{CB} is the pull-off force in the bumpy (nonadhesive, heated) state, with $F_{CF} > F_{CB}$ and $0 \leq S \leq 1$. For $S = 0$, there is no change in pull-off force, while $S = 1$ corresponds to an optimal switching action. The normalized pull-off forces (relative adhesion) and the switching efficiency were evaluated for all samples and tested temperatures, and are shown in **Figure 3**. As can be seen in Figure 3a the relative adhesion remains within one standard deviation of 1.00 for all samples up to temperatures of 60 °C. Increasing the temperature to 80 °C leads to a large drop in relative adhesion for both of the TWSME surfaces. This corresponds directly with the formation of protrusions on the NiTi TWSME surfaces at A_f (76 °C), which is just below 80 °C. The drop in relative adhesion remains stable up to 100 °C. The structured hybrid system shows no remaining adhesion force after the topographic change and the smooth hybrid system drops to half of its former adhesive force. In contrast to these TWSME hybrid systems, the reference system without TWSME, meaning without any switchable topography, shows no significant change in adhesion for all temperatures. Upon cooling and acclimating to room temperature, the NiTi TWSME surfaces return to ≈1.0 relative adhesion, corresponding to the protrusions returning to a flat surface.

Figure 3b shows the sample with the smooth PDMS layer has a switching efficiency S of 0.5 ± 0.02, while the patterned sample shows the strongest effect with a switching efficiency of 0.95 ± 0.05, resembling a near perfect switch within the measurement accuracy. The reference measurement with the NiTi-PDMS sample without TWSME demonstrates a low switching efficiency of 0.06 ± 0.03.

2.2. Modeling and Finite Element Analysis (FEA): Change in Contact Area

Multiple adhesion theories are available for the contact of elastic spheres.[20] The primary approaches have been proposed by Hertz,[21] Johnson et al. (JKR),[22] Derjauguin et al. (DMT),[23]

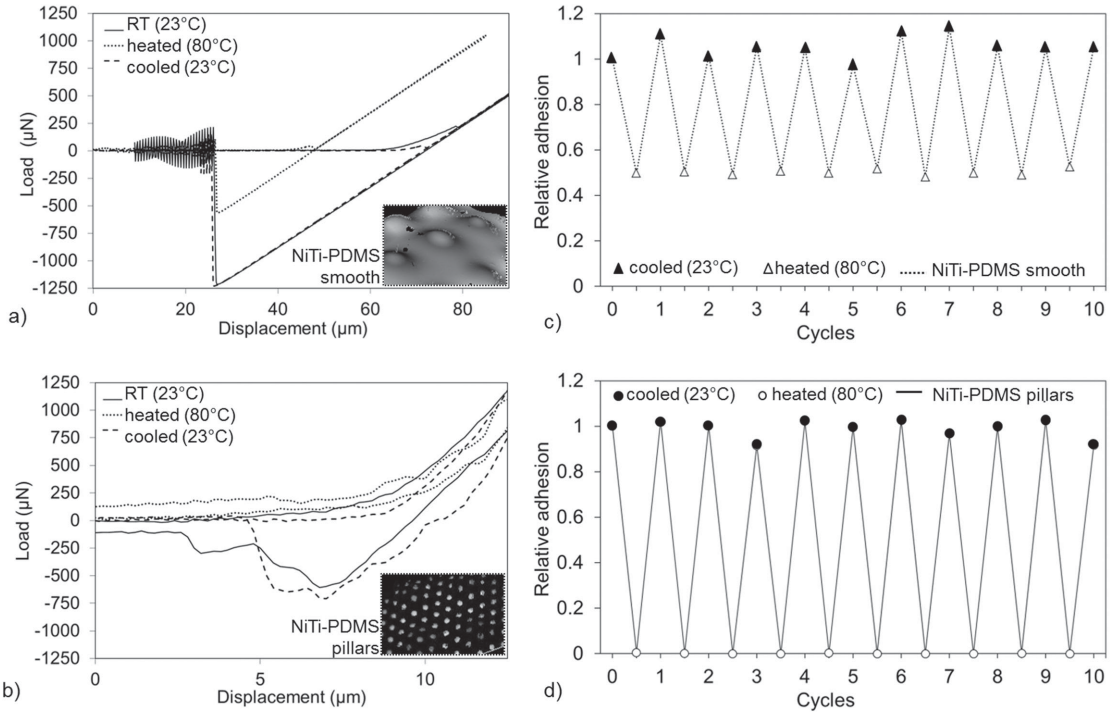

Figure 2. Adhesive performance and reversible switching of the two PDMS-hybrid systems. a,b) Representative load-displacement measurements for each system taken at room temperature, in the heated state at 80 °C and after cooling again to room temperature; the insets represent the topography of the samples in the heated state. c,d) The repeatability of switching between the adhesive and less/nonadhesive state. Adhesion is measured for 10 cycles from 23 to 80 °C. The value for relative adhesion is obtained by dividing the adhesion values by the initial adhesion value prior to thermal cycling.

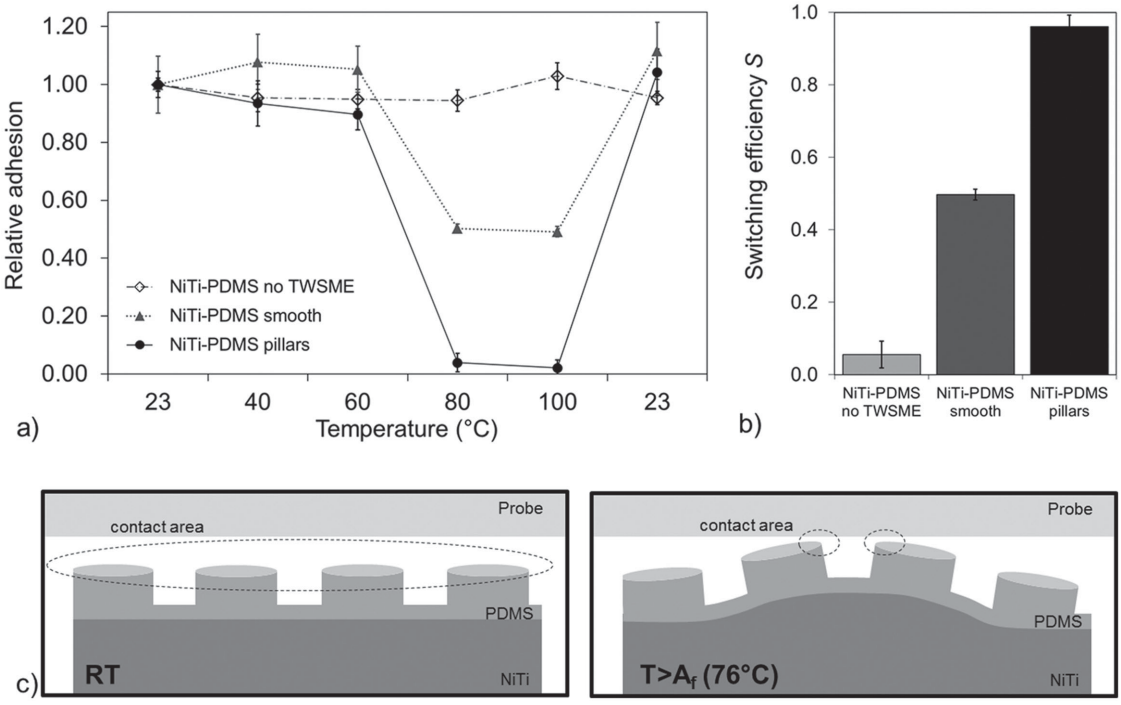

Figure 3. a) Change in adhesion with temperature. Relative adhesion, normalized by the room temperature value, is shown for the tested NiTi-PDMS hybrid systems and compared to the reference sample NiTi-PDMS hybrid without a TWSME. Adhesion is shown at different temperatures relative to the initial adhesion force. Lines are added to guide the eye. b) The calculated switching efficiency for the three tested systems. c) Schematic illustration of a patterned sample in the cooled and heated stage during adhesion test with a spherical probe, exemplifying the decrease in contact area. The dimensions of the protrusions are not to scale.

Maugis,[24] and Bradley.[25] Although these theories often times leads to very similar solutions, the appropriate theory for any particular application can be determined by the evaluation of two parameters. The first, μ, is a ratio of the elastic displacement of the surfaces at the point of pull-off to the effective range of the surface forces. This ratio is given by[20]

$$\mu = \left(\frac{Rw^2}{\left(E^*\right)^2 z_0^3} \right)^{1/3} \tag{2}$$

where R is the reduced radius of the spheres give by

$$R = \left(\frac{1}{R_1} + \frac{1}{R_2} \right)^{-1} \tag{3}$$

E^* is the combined elastic modulus of the spheres given by

$$E^* = \left(\frac{\left(1-\nu_1^2\right)}{E_1} + \frac{\left(1-\nu_2^2\right)}{E_2} \right)^{-1} \tag{4}$$

w is the work of adhesion (experimentally determined to 39 mJ m^{-2} for PDMS-glass adhesion), and z_0 is the equilibrium separation (taken to be 0.2 nm, which is the van der Waals radius of Si[26]). R_1 and R_2 are the radii of the two spheres and E and ν correspond to their Young's modulus and Poisson's ratio, respectively. The effective radius (R) for the flat specimen R_{CF} is 2.00 mm and the effective radius for the bumpy specimen R_{CB} is 0.806 mm, the radius of the bump was computed at the peak. Using geometric parameters given in **Table 1** and material properties given in **Table 2**, the values of μ for indentation of a flat surface and curved surface are given by 37.6 and 22.0, respectively. According to Johnson and Greenwood,[20] these values place the appropriate adhesion model as either JKR or Hertz, depending on the load. The critical parameter for determining between JKR and Hertz is the ratio $\overline{P}$ of load to pull-off force

$$\overline{P} = \frac{P}{\pi w R} \tag{5}$$

For indenting the flat and curved specimens at a load of 1000 μN these ratios are 4.1 and 20.2, respectively. These values place the adhesion studied here well within the JKR region of the adhesion map given by Johnson and Greenwood.[20]

Using JKR theory the pull-off force F is dependent only on the surface energy and the effective radius R

Table 1. Geometric parameters for finite element model.

Geometric parameter	[μm]
Indenter radius	2000
PDMS layer thickness	12
Bump height	3
Bump period	400
Model radius	75
Bilayer substrate thickness	47

Table 2. Material properties for finite element model.

	Glass[30]	PDMS[31]	NiTi[32]
E [GPa]	80	2.1	56
ν	0.3	0.49	0.3

$$F = -\frac{3}{2}\gamma\pi R \tag{6}$$

Thus, the JKR predicted switchability is given by

$$S_{JKR} = 1 - \frac{R_{CB}}{R_{CF}} = 0.60 \tag{7}$$

This value is slightly higher than the experimentally observed value of 0.50 ± 0.02, however, this is to be expected as indenting perfectly on the peak of a bump represents the condition with the *least* contact area and, consequently, the highest switchability. Thus, Equation (7) represents an upper bound on the switchability.

Despite the maturity and convenience of JKR theory to describe adhesion, the applicability of JKR in the case of compliant layers on elastic substrates is a topic of current research.[27,28] The primary feature of JKR is to consider adhesive forces within the contact area, which can be considered as the summation of a Hertz contact area plus an area that arises due to interactive surface forces. The surface forces themselves are not influenced by the bilayer nature of the PDMS/NiTi, but the Hertz solution will be affected. Consequently, to confirm that the switchability observed between the flat and bumpy morphologies could be described by conventional JKR theory, a finite element (FE) model for the Hertzian contact area was developed in Abaqus.[29] Modeling approaches of this type have been commonly used to assess the effects of a thin layer on adhesion.[27] The goal of the FE analysis was to evaluate whether the bilayer morphology combined with underlying surface bumps was well-approximated by a Hertzian contact approximation in the load regime of interest (<1000 μN) such that the use of Johnson–Kendall–Roberts (JKR) model to predict switchability would be appropriate.[21,22] As such, the finite element model discussed below did not explicitly include adhesive forces, but focused instead on evolution of contact area.

Two primary configurations were modeled: i) glass sphere indenting a flat PDMS-NiTi bilayer and ii) glass sphere indenting a PDMS-NiTi bilayer with a bump. Simulations of these two configurations with a pure PDMS material substituted for the bilayer were also simulated for comparison. All models were axisymmetric with geometric parameters as described in Table 1. The bilayer structure was meshed with 62400 4-node reduced integration axisymmetric elements (CAX4R); the indenter was meshed with 65100 CAX4R elements. The bumpy surface was modeled as a sinusoid. Contact between the glass indenter and the PDMS layer was implemented using surface to surface discretization with small sliding. Tangential contact behavior was assumed to be frictionless. Normal contact was defined as hard contact and all contact constraints were enforced directly (in contrast to a penalty method). Nominal linear elastic material properties were

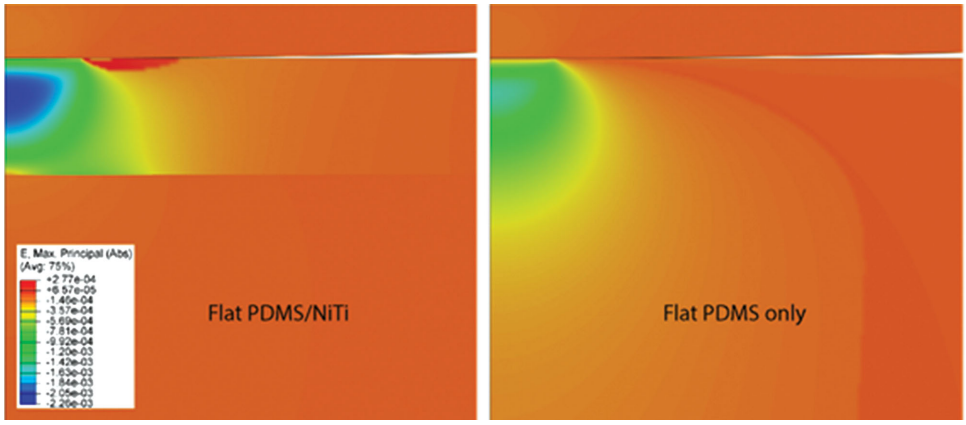

Figure 4. Maximum (absolute) principal strain for (left) bilayer specimen and (right) PDMS only specimen of the same geometry.

used for the three materials and are given in Table 2. Linear elastic material properties were selected because the von Mises stresses in the PDMS under the loads of interest did not exceed its yield strength. Loading was applied via displacement control on the top surface of the indenter and loads were computed from the summation of reaction forces on the top surface of the indenter. The bottom boundary of NiTi was fixed. To ensure convergence of the solution with contact nonlinearity, displacement incrementation was controlled such that the maximum displacement increment during any increment was 1 nm.

Contour plots of the maximum absolute principal strains at a load of 1000 μN for the flat specimen geometry are shown in **Figure 4**. The left is the bilayer specimen geometry; the right is the same geometry but with a substrate comprised completely of PDMS, shown for comparison as it represents the classic Hertz solution. The influence of the bilayer interface on the strain field can be clearly observed. In the bilayer material, the indent-induced strain is primarily contained in the more compliant PDMS layer such that the bilayer boundary serves to qualitatively change the morphology of the strain from the case of a homogeneous material. This is most evident in the region of the bilayer with a tensile strain component near the outside contact boundary; this is not observed in the homogeneous specimen.

The effect of the differences in strain morphology between the homogeneous PDMS material and the bilayer material on the contact area is not immediately obvious. To directly examine the differences, the contact area for the bilayer was computed via FE analysis as a function of load for both configurations. These data are shown in **Figure 5**a, where the dashed line is the contact area for the flat geometry and the solid curve is the contact area for the bumpy geometry. As expected, the contact area for the flat specimen is significantly larger than for the bumpy specimen (e.g., nearly a factor of two at the maximum preload). The Hertz contact area assuming a homogenous PDMS material was also calculated and is plotted for both configurations. The contact area after Hertz is given by[21]

$$A = \pi a^2 = \pi \sqrt[3]{\left(\frac{3FR}{4E^*}\right)^2} \tag{8}$$

where a is the radius of the contact area, F is the applied load, E^* is the effective modulus and defined in Equation (4), and R is the effective radius given by Equation (3).

For the Hertz contact calculation, the PDMS modulus only was used for the substrate and the NiTi was ignored. From Figure 5, the Hertz solution describes the contact area well for

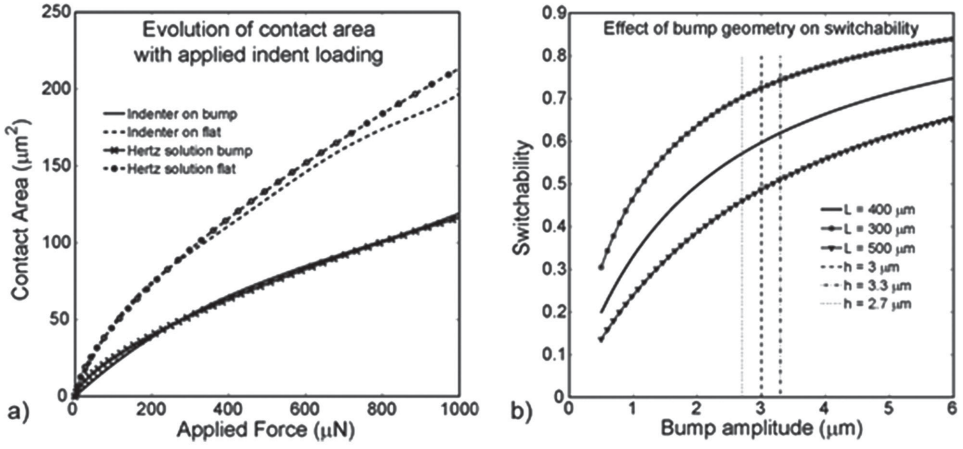

Figure 5. a) Evolution of contact area with applied load in a NiTi PDMS hybrid system. b) Effect of bump geometry on switchability.

both samples, but begins to deviate slightly with increasing load. The agreement between the finite element analysis (FEA) model of the bumpy bilayer sample and the Hertz PDMS-only model is very good. This indicates that although the interface does influence the stress and strain fields underneath the indenter, the analytical contact area calculation is still valid over the loads of interest. This was particularly surprising given the significant differences between the strains under the indenter due to the presence of the NiTi interface. Because of this good agreement with respect to contact area the use of analytical solutions, specifically JKR theory, to describe adhesion and switchability in this bilayer system is warranted.[22]

To examine the sensitivity of switchability to the geometry of the bump, Equation (4) was solved for bump amplitudes ranging from less than 1 up to 6 μm. In addition the period L of the bumps was varied from 300 to 500 μm. These results are shown in Figure 5b, where the dashed line indicates the value at which the FEA analysis was run (3 μm) and two lines showing ±10% of this value.

As can be seen from these data, the experimental values are well within predicted switchability bounds defined by uncertainties in the geometry. These comparisons are sufficient to conclude that the switchability is entirely due to geometry change and the resultant contact area reduction.

2.3. Topographic Change and PDMS Micropattern

The overarching goal of this research was to create a temperature-induced switchable adhesive surface. The premise was to utilize the recently discovered indentation-induced TWSME surfaces to change the contact area between the surface and the probe as a function of temperature. After cooling the flat surface would have a relatively large contact area with the probe, and after heating the structured surface would make poor contact (e.g., Figure 3c). These NiTi TWSME surfaces are advantageous because the change in surface structure occurs over a narrow temperature range, each state is stable at room temperature, is inherent to the material occurring very quickly (i.e., fraction of a second), and is repeatable over many thermal cycles. Furthermore, although not explored in this work, it would be possible to thermally cycle the NiTi relatively quickly using resistive heating.

Because metallic surfaces are well known to exhibit poor dry adhesion via van der Waals forces, our surfaces were coated with PDMS and PDMS pillars in order to facilitate contact adhesion.

The experimental investigation of our switchable adhesive surfaces revealed that the pull-off forces, switching efficiency, and reversibility of all tested samples are not only affected by the change in contact area but also by the topographic change of the TWSME material and the PDMS micropattern. Both factors are thoroughly discussed below in turn.

The results in Figure 3 strongly suggest that the switchability is due to the change in topography, caused by the TWSME of the NiTi alloy. This is supported by the fact that the NiTi-PDMS sample without TWSME shows no sudden switching behavior. Consequently, the temperature range at which the adhesion switch occurs may be adjusted by choosing a shape-memory alloy with a different transition temperature.

The sudden change in the adhesion at the transition temperature can be explained by the change in contact area between the surface and the probe induced by the TWSME of the NiTi (Figure 4c). The contact area between probe and sample is reduced due to the topographical changes of the NiTi and depends on the protrusion geometry, i.e., the width and the height.

Relative to a smooth PDMS coating, adding 50 μm diameter PDMS pillars on the NiTi TWSME surfaces had a dramatic influence on the adhesive behavior. At low temperatures, where the underlying NiTi is relatively flat, the addition of the pillars decreases the overall pull-off force. This is expected as the presence of the pillars will lead to an overall decrease in the contact area. It is difficult to quantify this value as the precise location of the probe on the surface will strongly influence the number of pillars it comes in contact with. Careful observation of the force-displacement curves in Figure 2b shows discontinuous behavior, indicating that multiple detachment events occur (i.e., pillars separate from the probe at different times). The approximately half-dozen discontinuities are consistent with the likely number of pillars in contact with the probe. Figure 2b also shows almost no measurable adhesion after heating. The reason for this drastic change in switching efficiency is most likely caused by the angle dependent adhesion of the pillar structures; it was shown that adhesion is greatly reduced if the tip of the structure and the probe are misaligned.[18] Even a very small tilt angle of 2°–3° causes a significant decrease in pull-off force. Furthermore, the inclination of the pillars due to the formation of protrusions will provoke bending of the pillars, which also reduces adhesion.[33] In this study the PDMS pillars were specifically designed to be shorter than their diameter. It is expected that long aspect ratio pillars may better conform to a rigid probe, and thereby increase contact area, as has been observed in previous studies.[34] In a subsequent study, this system will be modified using different adhesion enhancing tip geometries such as mushroom shaped tips or higher aspect ratios to further increase adhesion while maintaining the switchability.

3. Conclusions

In conclusion, we developed a switchable adhesion system by combining a NiTi two-way shape-memory alloy with a bioinspired adhesive PDMS layer. This hybrid material enables to reversibly switch between an adhesive and a low and nonadhesive state. By changing the protrusion geometry of the NiTi shape-memory alloy and the pattern of the PDMS layer we were able to alter the switching efficiency, the pull-off forces, and the reversibility of the switch. Such novel smart adhesives can be of interest for many applications such as pick and place processes, for temporary adhesion in biomedical devices, or for climbing robots. Furthermore, systems combining active shape-memory alloys and a functional surface may also be adapted to switch other surface properties, e.g. friction, wetting behavior or reflectivity. By use of an additional active material such as liquid crystal elastomers or shape memory polymers further functionality might be provided, triggered by one or two different stimuli, e.g., heat and/or UV-light.[35]

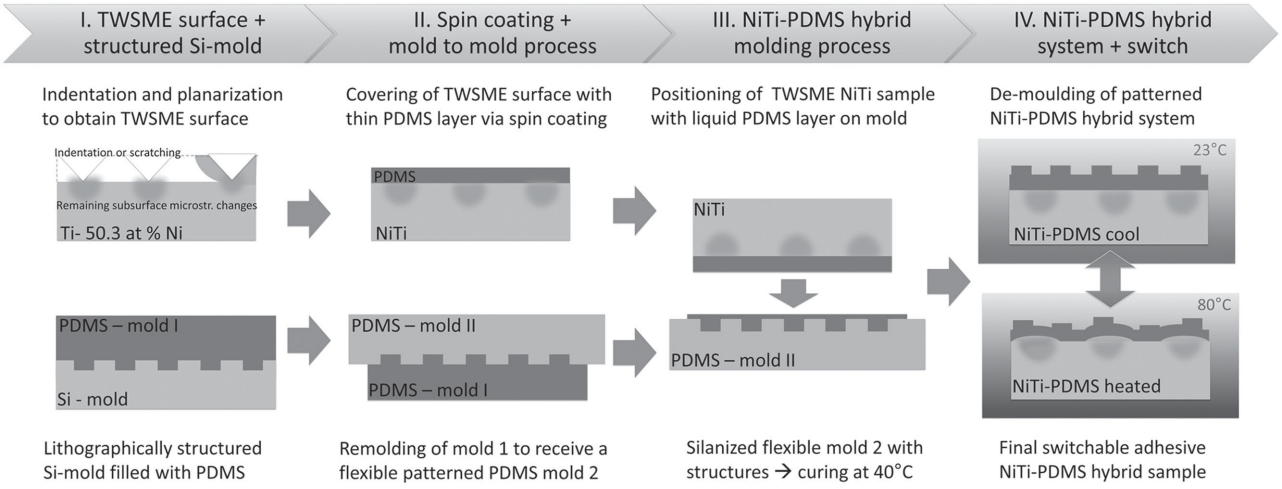

Figure 6. Schematic illustration of the fabrication process of the NiTi-PDMS hybrid system. The samples with a smooth PDMS layer on top were fabricated via spin coating. For the sample with a patterned PDMS layer a multiple step process was applied. A silicon wafer was patterned by photolithography, resulting in cylindrical cavities having a diameter of 50 µm and a depth of 40 µm. A PDMS mold I was cast from the structured silicon wafer and used as template to prepare a flexible PDMS mold II. The latter was applied for the final patterning of the PDMS layer on the hybrid system. Mold II was filled with liquid PDMS, and then a previously indented and polished NiTi sample was brought into contact with the filled mold. All hybrid systems were placed in an oven at 40 °C for 48 h to ensure full curing of the PDMS. The pillar patterned samples were carefully demolded to avoid delamination of the PDMS layer from the NiTi sample.

4. Experimental Section

Materials: In this study, a polycrystalline NiTi shape memory alloy (Ti-50.3 at% Ni (Ti-55.47 wt% Ni)) procured from Memry GmbH (Germany) was used. The alloy had a martensite finishing temperature (M_f) of about 25 °C and an austenite finishing temperature (A_f) of about 76 °C, as measured by differential scanning calorimetry. Thus, the material is expected to be martensite at room temperature, and austenite in the heated state at 76 °C and above. At temperatures in between, both states are stable depending on the thermal history of the material. For sample preparation, ⟨100⟩ silicon wafers were purchased from Crystec GmbH (Germany). The silanization was conducted with Hexadecafluoro-1,1,2,2-tetrahydrooctyltrichlorosilane acquired from AlfaAesar (MA, USA). Polydimethylsiloxane (PDMS, Sylgard 184) was purchased from Dow Corning (MI, USA). The negative photoresist SU8 and the developer mr-600 were procured from MicroChem GmbH (Germany).

Sample Preparation: NiTi bulk material of 2 mm thickness was cut into pieces of 10 × 10 mm. The two way shape memory NiTi surfaces were prepared by indentation with a hardness tester (type V-100-C1, LecoInstrumente, Germany) and a Vickers diamond indenter tip (Ahotec, Germany). A 32 × 65 matrix of indents with interspaces of 400 µm was produced with a load of 10 N. Indentation was performed at ≈–50 °C. After deformation, the samples were replanarized via multistep grinding with SiC paper and mechanical polishing down to 0.25 µm diamond paste. The remaining deformation layer was removed by electropolishing (PoliMat2, Buehler, Germany) with 20 vol% H_2SO_4 and 80 vol% methanol electrolyte solution at 13 V for 60 s. The indented and planarized NiTi samples were covered with a 10–15 µm thick layer of PDMS by spin-coating (type CT62, Karl Suss, Germany). The base and crosslinker of PDMS were mixed in a ratio of 10:1, degassed in a desiccator, and poured onto the NiTi sample with subsequent spinning at 5000 rpm for 200 s. The PDMS layer was cured for 48 h at 40 °C (T < As). As reference sample a NiTi-PDMS hybrid system without TWSME was prepared using the same protocol. The samples with a patterned PDMS layer were prepared in a two-step process (**Figure 6**). i) The NiTi alloy was indented and polished as described above and covered with an about 10 µm PDMS layer via spin-coating. ii) A silicon wafer was spin-coated with SU8, heat treated at 65 and 95 °C, exposed to UV-light (365 nm) through a lithography mask (ML&C Jena GmbH, Germany) and subsequently developed, resulting in arrays of holes with 50 µm diameter and a depth of 40 µm. The silicon wafer was replicated by mixing PDMS in a 10:1 ratio, degassing, pouring the liquid PDMS onto the silicon mold and curing at 75 °C for 12 h, resulting in PDMS mold (I), which was subsequently silanized. To prevent stiction to the mold and facilitate the demolding process of the hybrid system the silicon mold was silanized by vapor deposition of the silane (hexadecafluoro-1,1,2,2-tetrahydrooctyltrichlorosilane) in a desiccator for 40 min and subsequently heat treated at 95 °C for 45 min.[34] The process was repeated, using PDMS mold (I) as master mold, achieving PDMS mold (II). The PDMS mold (II) was filled with mixed and degassed PDMS, merged with the sample from process step (i) and cured in an oven at 40 °C for 48 h. Finally, the flexible PDMS mold (II) was carefully removed from the sample. The topography of both samples was measured in the initial state at room temperature, after heating to 80 °C and after cooling again to room temperature using white light interferometry (ZygoNewView 5000, Zygo, USA) and inverse optical microscopy (Olympus PMG3, Olympus Corporation, Japan). The profiles of ten representative protrusions were measured for each sample in the heated state before and after covering the surface with PDMS. The arithmetical mean and standard deviations where calculated for their heights and diameters.

Adhesion Measurements: Adhesion was measured with a custom-built adhesion tester. The positioning stage was equipped with a heating element. A spherical 4 mm diameter glass probe was fixed to the cantilever, measuring deflection by laser interferometry, further details are described in ref.[36] The spring constants of the double beam glass spring were k = 284 N m^{-1} for the samples with a smooth PDMS layer and k = 2475 N m^{-1} for the patterned sample. All measurements were performed using a constant displacement velocity of 5 µm s^{-1}. Adhesion was measured at least ten times for each temperature. The tests were performed at about 10 mN for the sample with the smooth PDMS layer and about 15 mN for the patterned sample, where pull off force was found to be independent of preload. For temperature cycling, ten measurements were performed on each sample at three positions in the cooled and heated state. An arithmetical mean and standard deviations were calculated from the pull-off forces.

Acknowledgements

The research leading to these results has received funding from the European Research Council under the European Union's Seventh Framework Program (FP/2007–2013)/ERC Grant Agreement No. 340929. C.P.F. gratefully acknowledges the support of this work from the National Science Foundation (NSF) CAREER award (Grant No. DMR-1255603) as well as the University of Wyoming International Travel Grant.

Received: February 2, 2015
Revised: March 16, 2015
Published online: April 8, 2015

[1] a) A. del Campo, E. Arzt, *Chem. Rev.* **2008**, *108*, 911; b) D. Sameoto, C. Menon, *Smart Mater. Struct.* **2010**, *19*, 103001; c) L. F. Boesel, C. Greiner, E. Arzt, A. del Campo, *Adv. Mater.* **2010**, *22*, 2125.
[2] K. Autumn, A. Dittmore, D. Santos, M. Spenko, M. Cutkosky, *J. Exp. Biol.* **2006**, *209*, 3569.
[3] a) M. P. Murphy, B. Aksak, M. Sitti, *J. Adhes. Sci. Technol.* **2007**, *21*, 1281; b) M. P. Murphy, B. Aksak, M. Sitti, *Small* **2009**, *5*, 170; c) M. Kamperman, E. Kroner, A. del Campo, R. M. McMeeking, E. Arzt, *Adv. Eng. Mater.* **2010**, *12*, 335.
[4] M. J. Vogel, P. H. Steen, *Proc. Natl. Acad. Sci. U. S. A.* **2010**, *107*, 3377.
[5] A. G. Gillies, J. Kwak, R. S. Fearing, *Adv. Funct. Mater.* **2013**, *23*, 3256.
[6] M. T. Northen, C. Greiner, E. Arzt, K. L. Turner, *Adv. Mater.* **2008**, *20*, 3905.
[7] D. Paretkar, M. Kamperman, A. S. Schneider, D. Martina, C. Creton, E. Arzt, *Mater. Sci. Eng., Proc. Conf.* **2011**, *31*, 1152.
[8] N. Nadermann, J. Ning, A. Jagota, C. Y. Hui, *Langmuir* **2010**, *26*, 15464.
[9] H. E. Jeong, M. K. Kwak, K. Y. Suh, *Langmuir* **2010**, *26*, 2223.
[10] J. Krahn, D. Sameoto, C. Menon, *Smart Mater. Struct.* **2011**, *20*, 015014.
[11] S. Kim, M. Sitti, T. Xie, X. Xiao, *Soft Matter* **2009**, *5*, 3689.
[12] J. D. Eisenhaure, T. Xie, S. Varghese, S. Kim, *ACS Appl. Mater. Interfaces* **2013**, *5*, 7714.
[13] S. Reddy, E. Arzt, A. del Campo, *Adv. Mater.* **2007**, *19*, 3833.
[14] a) A. Nagasawa, K. Enami, Y. Ishino, Y. Abe, S. Nenno, *Scr. Metall.* **1974**, *8*, 1055; b) K. Otsuka, T. Kakeshita, *MRS Bull.* **2002**, *27*, 91.
[15] a) W. Ni, Y.-T. Cheng, D. S. Grummon, *Surf. Coat. Technol.* **2004**, *177*, 512; b) Y. Zhang, Y.-T. Cheng, D. S. Grummon, *Appl. Phys. Lett.* **2006**, *88*, 131904.
[16] X. Fei, Y. Zhang, D. S. Grummon, Y.-T. Cheng, *J. Mater. Res.* **2009**, *24*, 823.
[17] E. Qin, N. J. Peter, M. Frensemeier, C. P. Frick, E. Arzt, A. S. Schneider, *Adv. Eng. Mater.* **2014**, *16*, 72.
[18] E. Kroner, E. Arzt, *Int. J. Adhes. Adhes.* **2012**, *36*, 32.
[19] G. Guidoni, D. Schillo, U. Hangen, G. Castellanos, E. Arzt, R. McMeeking, R. Bennewitz, *J. Mech. Phys. Solids* **2010**, *58*, 1571.
[20] K. L. Johnson, J. A. Greenwood, *J. Colloid Interface Sci.* **1997**, *192*, 326.
[21] H. Hertz, *J. Reine Angew. Math.* **1881**, *92*, 110.
[22] K. L. Johnson, K. Kendall, A. D. Roberts, *Proc. R. Soc. A* **1971**, *324*, 301.
[23] a) B. V. Derjaguin, V. M. Muller, Y. P. Toporov, *J. Colloid Interface Sci.* **1975**, *53*, 314; b) M. D. Pashley, *Colloids Surf.* **1984**, *12*, 69.
[24] D. Maugis, *J. Colloid Interface Sci.* **1992**, *150*, 243.
[25] R. S. Bradley, *Philos. Mag.* **1932**, *13*, 853.
[26] A. Bondi, *J. Phys. Chem.* **1964**, *68*, 441.
[27] a) I. Sridhar, K. L. Johnson, N. A. Fleck, *J. Phys. D: Appl. Phys.* **1997**, *30*, 1710; b) K. L. Johnson, I. Sridhar, *J. Phys. D: Appl. Phys.* **2001**, *34*, 683; c) I. Sridhar, Z. W. Zheng, K. L. Johnson, *J. Phys. D: Appl. Phys.* **2004**, *37*, 2886; d) R. Sburlati, *Int. J. Solids Struct.* **2009**, *46*, 975; e) E. D. Reedy, *J. Mater. Res.* **2006**, *21*, 2660.
[28] E. Barthel, A. Perriot, *J. Phys. D: Appl. Phys.* **2007**, *40*, 1059.
[29] SIMULIA, Dassault Systemes, **2014**.
[30] W. C. Oliver, G. M. Pharr, *J. Mater. Res.* **1992**, *7*, 1564.
[31] a) F. Carrillo, S. Gupta, M. Balooch, S. J. Marshall, G. W. Marshall, L. Pruitt, C. M. Puttlitz, *J. Mater. Res.* **2005**, *20*, 2820; b) G. Castellanos, E. Arzt, M. Kamperman, *Langmuir* **2011**, *27*, 7752.
[32] Y. Liu, H. Xiang, *J. Alloys Compd.* **1998**, *270*, 154.
[33] D. Paretkar, M. Kamperman, D. Martina, J. Zhao, C. Creton, A. Lindner, A. Jagota, R. McMeeking, E. Arzt, *J. R. Soc. Interface* **2013**, *10*, 20130171.
[34] C. Greiner, A. del Campo, E. Arzt, *Langmuir* **2007**, *23*, 3495.
[35] D. Liu, D. J. Broer, *Angew. Chem. Int. Ed.* **2014**, *53*, 4542.
[36] E. Kroner, J. Blau, E. Arzt, *Rev. Sci. Instrum.* **2012**, *83*, 016101 .